

**Generalized effective-medium model for the carrier mobility in amorphous organic semiconductors**Vadim Rodin,<sup>1,\*</sup> Franz Symalla,<sup>2</sup> Velimir Meded,<sup>2</sup> Pascal Friederich,<sup>2</sup> Denis Danilov,<sup>2</sup> Angela Poschlad,<sup>3</sup> Gabriele Nelles,<sup>1</sup> Florian von Wrochem,<sup>1</sup> and Wolfgang Wenzel<sup>2</sup><sup>1</sup>*Materials Science Laboratory, SONY Deutschland GmbH, Hedelfinger Strasse 61, D-70327 Stuttgart, Germany*<sup>2</sup>*Institute of Nanotechnology, Karlsruhe Institute of Technology (KIT), D-76021 Karlsruhe, Germany*<sup>3</sup>*Steinbuch Centre for Computing, Karlsruhe Institute of Technology (KIT), D-76021 Karlsruhe, Germany*

(Received 9 December 2014; revised manuscript received 5 March 2015; published 10 April 2015)

Electronic transport through disordered organic materials is relevant in many applications, including organic light-emitting diodes and organic photovoltaics. The charge-carrier mobility is one of the most important material characteristics that must be optimized to make organic devices competitive. Here we introduce a general effective-medium model for the analytic calculation of zero-field mobilities on the basis of material-specific parameters that are obtained from extensive *ab initio* simulations. By means of kinetic Monte Carlo simulations, we generalize the model to also include the strong disorder limit. As a proof of concept the model is applied to two different disordered organic materials exhibiting medium and strong disorder, respectively. Surprisingly, even at strong disorder the hole mobilities computed with the effective-medium model in its original form are found to agree best with the experimental data. Seeking a possible explanation for this result, we investigate the strong dependence of the mobility on the connectivity of the model topology and show that the distribution of hopping matrix elements in the material is indeed much broader than assumed in simple lattice models. As the input parameters of the model can be computed on the basis of relatively small samples, this model may be used for materials' screening without adjustable parameters.

DOI: [10.1103/PhysRevB.91.155203](https://doi.org/10.1103/PhysRevB.91.155203)

PACS number(s): 72.80.Le, 71.23.-k, 72.20.Ee

**I. INTRODUCTION**

Driven both by the fundamental research and by the current level of applications there has been strong interest in transport properties of thin-film materials, which are used in organic light-emitting diodes [1], organic photovoltaics [2,3], or organic field effect transistors [4]. However, the theoretical prediction of their functional properties still remains a challenge [5,6]. At room temperature, ordered organic semiconductors show relatively high carrier mobilities (e.g.,  $\mu \simeq 1 \text{ cm}^2 \text{ V}^{-1} \text{ s}^{-1}$  [7], cf.  $\mu \simeq 10^2 - 10^4 \text{ cm}^2 \text{ V}^{-1} \text{ s}^{-1}$  for crystalline inorganic semiconductors [8]). The mobilities in disordered amorphous molecular systems and polymers are typically three to five orders of magnitude lower than in crystals [9,10].

Motivated by relevance of these materials for organic electronics applications, a number of models have been developed to understand [11–13] and to predict [14–17] charge-carrier mobility in disordered organic materials, but no compact expression for the mobility, using input from first-principles calculations, has been derived to date. For a parameter-free prediction of the intrinsic mobility, material-specific microscopic parameters, such as the spatial distribution of hopping sites, the distribution of site energies, and the hopping matrix elements, must be linked to transport theories. Recently, kinetic Monte Carlo (KMC) methods have widely been used to compute the mobility, in part because material-specific microscopic parameters can easily be integrated [6,14,16,18–20]. However, these methods require large lattice sizes in the limit of strong disorder and struggle to represent the local coordination of the hopping sites. Charge transport in disordered semiconductors is intimately

related to the percolation problem [21–23] of conducting pathways. Based on this concept, a scaling transport theory has been developed [24–26], which parametrizes the mobility depending on the lattice type and the degree of the energy correlation. The parameters of these models are typically fit by comparison with experimental data. In addition, there have been recent efforts to compute relevant parameters for mobility models from first-principles calculations [14,16,20,27], and it would be desirable to develop transport models that can directly use these parameters to compute the macroscopic observables of the system.

In this paper we attempt one step in this direction. We begin by developing a generalized effective-medium model (GEMM) that directly uses microscopic parameters obtained from *ab initio* calculations of the bulk morphology of organic materials. This model yields an analytic upper bound on the zero-field bulk mobility of disordered materials and hence cannot describe the percolation limit. As a next step, we fit the exponent of the GEMM that describes the dependence of mobility on the energy disorder to reproduce the strong disorder limit by comparing to lattice KMC data. We then test the GEMM by comparing its results with experimental data for two specific materials, namely, tris-(8-hydroxyquinoline)aluminum (Alq<sub>3</sub>) and *N,N'*-bis(1-naphthyl)-*N,N'*-diphenyl-1,1'-biphenyl-4,4'-diamine ( $\alpha$ -NPD), which strongly differ in their energy disorders [13], and finally analyze the results.

**II. METHODS****A. Master equation**

Hopping transport can be described by a master-equation (ME) approach [28] where each molecule represents a hopping site and the probability  $p_i$  to find a carrier on the site  $i$  at time

\*Vadim.Rodin@eu.sony.com

$t$  evolves according to

$$\frac{dp_i}{dt} = \sum_j p_j \omega_{ji}(1-p_i) - p_i \omega_{ij}(1-p_j) \quad (1)$$

with  $\sum_i p_i = N_c$  being the total number of charge carriers and  $\omega_{ij}$  being the rate of the transition from  $i$  to  $j$ . Site positions can be approximated by lattices [29] or by realistic distributions of molecules derived from atomistic simulations [14–16]. In heuristic models, e.g., the Gaussian disorder model (GDM), the energetic disorder is described in terms of the variance  $\sigma$  of the (Gaussian) density of states (DOS). However, no direct connection between heuristic models and first-principles electronic structure calculations has been demonstrated so far [30–32].

The mobility is then evaluated from the steady-state solution of the ME, which can be obtained by directly solving Eq. (1) for low carrier densities [33], or by a numerical solution using the KMC method. In the latter approach, the drift-diffusion trajectory of charge carriers is tracked in order to determine the time needed to move from one side of the sample to the other by hopping, depending on the magnitude of the applied external field. This emulates experimental time-of-flight measurements of the mobility [13]. A popular expression for the mobility,

$$\mu \propto \exp(-C\beta^2\sigma^2) \quad (2)$$

with  $C \approx 0.44$ , was obtained by Bässler [11] as a fit to his numerical KMC data for medium energy disorder [ $2 < \beta\sigma < 6$ , and  $\beta = 1/(k_B T)$  is the reciprocal temperature].

In the following section a GEMM is introduced. In the model the zero-field mobility is derived in the low charge-carrier density limit from the response of a system of charge carriers, being initially in thermal equilibrium in a macroscopic sample, to an instantaneous switching on of the electric field. This approach allows one to determine the zero-field mobility in the effective-medium limit within the nondispersive hopping transport regime as an intrinsic material property.

A necessary condition for the existence of a steady drift is that the mean carrier velocity remains constant for a sufficiently long time, during which the carriers drift a characteristic distance in the system (which may be the mean hopping distance in a disordered semiconductor). If the steady flow of carriers would set in immediately as the electric field is switched on at  $t = 0$ , then the initial value of the average velocity would be directly proportional to the zero-field mobility. We rigorously show (see Appendix B) that the initial velocity provides an exact upper bound on the intrinsic zero-field mobility, which we find to be in surprisingly good quantitative agreement with the experimental data. As we demonstrate below, this approximation breaks down in the percolation limit, i.e., for high disorder *and* low coordination.

## B. Derivation of GEMM's expression for the zero-field mobility

In thermal equilibrium the occupation probabilities  $p_i^{(0)}$  of charge carriers are given by the Fermi-Dirac distribution function  $p_i^{(0)} = \{1 + \exp[\beta(\epsilon_i - \mu)]\}^{-1}$ , where  $\epsilon_i$  is the site energy and  $\mu$  is the chemical potential. This provides a fundamental steady-state solution of the ME [see Eq. (1)],

holding due to the detailed balance of the thermally averaged rates,

$$\Gamma_{ji}^{(0)} = \Gamma_{ij}^{(0)}, \quad \Gamma_{ij}^{(0)} = p_i^{(0)} \omega_{ij}^{(0)} (1 - p_j^{(0)}). \quad (3)$$

An instantaneous switching on of a homogeneous electric field  $\vec{F} = 0$  ( $t < 0$ ),  $\vec{F} \neq 0$  ( $t \geq 0$ ) brings the system out of equilibrium. In Eq. (1),  $\omega_{ji} = \omega_{ji}^{(0)} + \Delta\omega_{ji}$  are now the new rates in the presence of the field (the change  $\Delta\omega_{ji}$  is not assumed small). The corresponding solution of the ME for  $t \geq 0$  may be written down as  $p_i(t) = p_i^{(0)} + \delta p_i(t)$ ,  $\delta p_i(0) = 0$  with  $\delta p_i$  satisfying the linearized ME for short times after  $t = 0$ ,

$$\frac{d\delta p_i}{dt} = \sum_j p_j^{(0)} \omega_{ji} (1 - p_i^{(0)}) - p_i^{(0)} \omega_{ij} (1 - p_j^{(0)}) + O(\delta p_i). \quad (4)$$

The mean drift velocity of the carriers at the time  $t = 0+$ , just after the switching on of the electric field, can be used to characterize the zero-field mobility,

$$\vec{v} = \frac{1}{2N_c} \sum_{ij} \Gamma_{ij}^{(0)} \left( \frac{\omega_{ji}}{\omega_{ji}^{(0)}} - \frac{\omega_{ij}}{\omega_{ij}^{(0)}} \right) \vec{r}_{ij} \quad (5)$$

Here,  $\vec{r}_{ij} = \vec{r}_i - \vec{r}_j$ , and  $\vec{r}_{ij}$  is the site radius vector. This expression in the zero-field limit yields the mobility tensor (see Appendix A for details),

$$\mu^{\alpha\gamma} = \frac{q\beta}{2N_c} \sum_{ij} \Gamma_{ij}^{(0)} r_{ij}^\alpha (r_{ij}^\gamma + d_{ij}^\gamma/q) \quad (6)$$

provided that the fluctuations in the induced local electric field can be neglected. Here  $q = \pm e$  is the carrier charge,  $\vec{d}_{ij} = \vec{d}_i - \vec{d}_j$ , and  $\vec{d}_i$  is the on-site dipole moment. When the contribution of  $\vec{d}_i$  in Eq. (6) can be neglected, Eq. (6) coincides with the Kasuya-Koide result [34,35], re-derived later by making use of a generalized master equation [36].

It is instructive to compare Eq. (6) with an ansatz [37,38] in which mobility is given by Einstein's relation  $\mu = e\beta D$  with the diffusion coefficient,

$$D = \frac{1}{2nN_0} \sum_{ij} P_{ij} \omega_{ij}^{(0)} r_{ij}^2 \quad (7)$$

where  $P_{ij} = \omega_{ij}^{(0)} / \sum_j \omega_{ij}^{(0)}$ ,  $N_0$  is the total number of sites, and  $n (= 1-3)$  is the effective spatial dimension of the transport. Equation (7) is adequate for systems with no disorder (crystalline materials) but leads to huge errors if strong disorder is present as the expression leads to effectively constant mobilities as a function of disorder (see a similar criticism by Stehr *et al.* [33]). By making use of Einstein's relation and Eq. (6) with  $\vec{d}_i = 0$ , an alternative expression, valid also for disordered materials, can be written down

$$D = \frac{1}{2nN_c} \sum_{ij} \Gamma_{ij}^{(0)} r_{ij}^2 \quad (8)$$

To calculate the hopping rates in Eq. (6), we employ here the commonly used Marcus rates [39–41],

$$\omega_{ij}^{(0)} = f_M \frac{J_{ij}^2}{\lambda^2} \exp \left[ -\beta \frac{(\epsilon_{ij}^- - \lambda/2)^2}{\lambda} \right]. \quad (9)$$

Here,  $J_{ij}$  are the hopping matrix elements,  $f_M = \frac{\sqrt{\pi\beta}}{h} \lambda^{3/2}$ , and  $\epsilon_{ij}^+ = (\epsilon_i + \epsilon_j)/2$ ,  $\epsilon_{ij}^- = (\epsilon_i - \epsilon_j)/2$  are the mean energies and the energy differences of the neighboring hopping sites. In the limit of low carrier concentrations one gets

$$\begin{aligned} \mu^{\alpha\gamma} &= \frac{q\beta f_M}{2N_0 \langle e^{-\beta\epsilon} \rangle} \sum_{ij} \frac{J_{ij}^2}{\lambda^2} \exp \left[ -\beta \left( \epsilon_{ij}^+ + \frac{\lambda}{4} + \frac{(\epsilon_{ij}^-)^2}{\lambda} \right) \right] \\ &\times r_{ij}^\alpha (r_{ij}^\gamma + d_{ij}^\gamma/q). \end{aligned} \quad (10)$$

If the energetic and spatial disorders are uncorrelated and the contribution of the on-site dipole moments is neglected, the zero-field mobility becomes

$$\mu_0 = \frac{e\beta f_M}{2n} \exp \left[ -\beta \frac{\lambda}{4} \right] \frac{\langle \exp[-\beta(\epsilon^+ + \frac{\epsilon^-^2}{\lambda})] \rangle}{\langle \exp[-\beta\epsilon] \rangle} M \frac{\langle J^2 r^2 \rangle}{\lambda^2}, \quad (11)$$

where  $M$  is the effective mean number of neighbors connected with a given site by nonzero transfer integrals  $J$  (analog to the “percolation correction factor” [42]).

For a Gaussian density of states the expression for the mobility in the zero-field and low-concentration limit is as follows:

$$\mu_0 = \frac{e\beta f_M}{2n\sqrt{1 + \frac{\beta\sigma^2}{\lambda}}} \exp \left[ -C(\beta\sigma)^2 - \beta \frac{\lambda}{4} \right] M \frac{\langle J^2 r^2 \rangle}{\lambda^2}, \quad (12)$$

with  $C = 0.25$ .

In the following we will refer to Eq. (12) as the main expression of the GEMM. We will use in Eq. (12) parameters  $\sigma$ ,  $\lambda$ , and  $J$  from *ab initio* models and various values of  $C$  to address also the percolation limit.

By calculating the mean carrier acceleration at  $t = 0$ , one can see that the charge is being decelerated, see Appendix B. Thus, strictly speaking, Eqs. (5) and (12) provide an exact upper bound for the zero-field mobility.

Analytical models for the charge-carrier mobility in an effective-medium approach have been reported before [43–45]. However, the derivation of the models as well as their final formulas somewhat differ from the ones of the present paper.

### C. Kinetic Monte Carlo

For a given model morphology of hopping sites, charge-carrier mobilities can be determined by explicitly simulating the microscopic hopping transport with the kinetic Monte Carlo method [11]. Molecules are representing hopping sites, which may or may not be on a lattice, interconnected by hopping rates that may be computed from Marcus theory or other models. Charge propagation through this lattice can then be simulated by iteratively drawing hopping events from the probability distribution of all possible events. For uncorrelated processes the time step of the event is determined

by  $t = \omega_{\text{tot}}^{-1} \ln(1/u)$ , where  $u$  is a random number drawn from a uniform distribution and  $\omega_{\text{tot}}$  is the sum of all rates. In the presence of an electric potential, the drift velocity of charge carriers is determined by the accumulated hopping distance in the field direction divided by the time passed. For our KMC calculations we employ Marcus rates as defined in Eq. (9) where the hopping matrix elements are parametrized as  $J_{if}^2 = e^{-2\alpha R_{if}}$  with  $2\alpha = 10/a$  on a simple cubic (SC) lattice with lattice constant  $a = 1$  nm and  $\lambda = 0.158$  eV (the value for  $\alpha$ -NPD, see Appendix C).

## III. RESULTS

### A. Percolation limit

It is clear that Eq. (12) can only describe the effective-medium limit in which percolation is not relevant. For increasing disorder the assumption that the finite-time site occupation probabilities correspond to their thermal zero time expectation values is no longer correct. Prior work has shown that the percolation regime can be captured by adjusting the parameter  $C$  in Eq. (12) depending on the details of the lattice coordination and correlation effects [12,24,26,41]. This is a reasonable approximation as the functional dependence of the mobility is by far strongest with respect to this parameter.

One approach to extend the model is therefore to fit it to KMC simulations. In Fig. 1, we compare Eq. (12) for three values of  $C$  with KMC data for simple cubic lattices with the typically assumed minimal coordination of 6. As expected we find that the effective-medium theory ( $C = 0.25$ ) and KMC agree only for small disorder, whereas the adjustment to  $C = 0.36$  is required to correctly fit to the KMC results for disorder strengths  $\beta\sigma = 1-5$ . The mobilities of the GEMM formula using Bässler’s prefactor  $C = 0.44$  in the exponent are

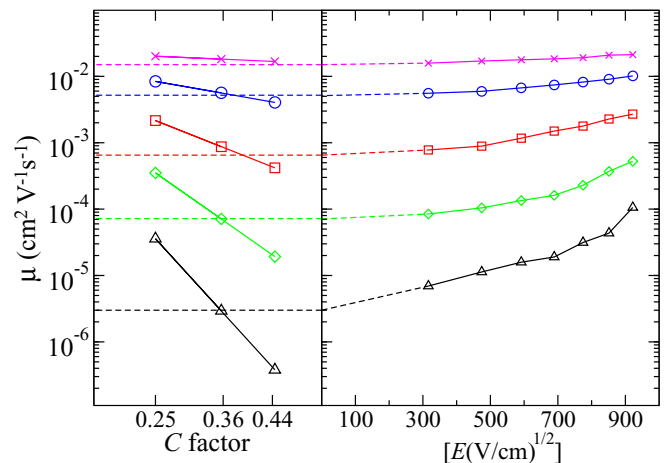


FIG. 1. (Color online) Left: zero-field mobilities of the GEMM for varying disorder strength  $\beta\sigma$  from 1 to 5 with  $C = 0.25, 0.36$ , and  $0.44$ , respectively; the dashed lines represent the KMC extrapolation to zero-field mobility. Right: KMC results for a simple cubic lattice with varying disorder strength  $\beta\sigma$  between 1 and 5 and a coordination of 6 as a function of the square root of the applied electric field. For  $0.44$  and  $0.25$  the discrepancy rapidly increases with increased disorder with  $0.44$  underestimating and  $0.25$  overestimating the mobility.  $C = 0.36$  provides the best fit to the KMC results.

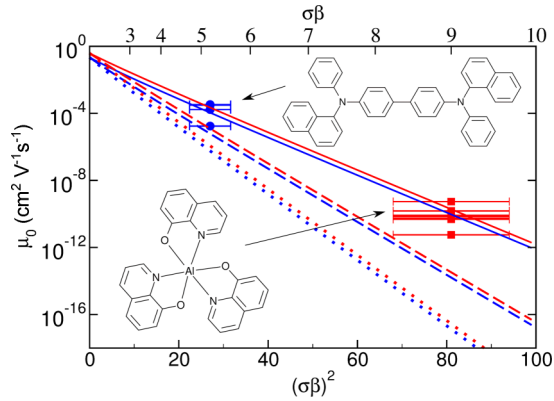


FIG. 2. (Color online) The dependence of zero-field hole mobilities Eq. (12) on the reduced disorder parameter  $(\beta\sigma)^2$  at  $T = 290$  K for the effective medium ( $C = 0.25$ , solid lines), the KMC ( $C = 0.36$ ), dashed lines), and Bässler's ( $C = 0.44$ , dotted lines) models for Alq<sub>3</sub> (red/top lines) and  $\alpha$ -NPD (blue/bottom lines). The circles denote experimental data for  $\alpha$ -NPD [46,47], and the squares denote experimental data for Alq<sub>3</sub> [46–50]. On the  $x$  axis the experimental data points are positioned at the corresponding calculated energy disorder. The horizontal error bars of the experimental data points illustrate the stochastic uncertainties of energy disorder resulting from the limited sample size of our microscopic input data. The insets display the chemical formulas of the corresponding materials.

presented too. The deviations of GEMM mobilities from KMC results are consistent with previous studies of the mobility dependence on the exponential prefactor in similar model systems [12,24].

### B. Zero-field mobility estimates for Alq<sub>3</sub> and $\alpha$ -NPD

In the following we calculate hole transport in amorphous Alq<sub>3</sub> and  $\alpha$ -NPD, both prototypical organic semiconductors. Microscopic parameters are calculated with a refined version (see Appendix C) of the previously reported quantum patch method [27], which calculates intermolecular polarization effects on a fully quantum-mechanical level. For Alq<sub>3</sub> we obtain values of  $J^2\tau^2 = 9.05 \times 10^{-3} \text{ eV}^2 \text{ \AA}^2$ ,  $\lambda = 0.213 \text{ eV}$ ,  $\sigma = 0.227 \text{ eV}$ , and  $M = 7.31$ , leading to a zero-field hole mobility of  $\mu_0 = 1.91 \times 10^{-10} \text{ cm}^2 \text{ V}^{-1} \text{ s}^{-1}$  at 290 K, very close to the experimental values [46–50]. For  $\alpha$ -NPD, we obtained values of  $J^2\tau^2 = 1.415 \times 10^{-3} \text{ eV}^2 \text{ \AA}^2$ ,  $\lambda = 0.158 \text{ eV}$ ,  $\sigma = 0.130 \text{ eV}$ , and  $M = 13.0$  which result in zero-field hole mobility  $\mu_0 = 1.11 \times 10^{-4} \text{ cm}^2 \text{ V}^{-1} \text{ s}^{-1}$  at  $T = 290$  K, again very close to the range of experimental values [46,47].

In Fig. 2 we have plotted  $\mu_0$  vs  $(\beta\sigma)^2$  from Eq. (12) for the rigorous upper limit from the effective-medium theory with  $C = 0.25$ , fitted to our KMC data ( $C = 0.36$ ) and Bässler's data ( $C = 0.44$ ). We observe an essentially linear dependence but note that the experimental data agree best with the effective-medium theory even for large disorder.

### C. Temperature dependence

We have further investigated the temperature dependence of the zero-field mobility as shown in Fig. 3. We show the temperature dependence of the zero-field hole mobilities

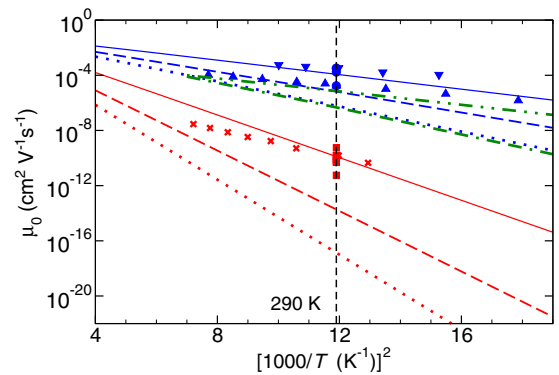


FIG. 3. (Color online) Temperature dependence of zero-field hole mobilities in Alq<sub>3</sub> (red/three bottom lines) and  $\alpha$ -NPD (blue/three top lines) according to the GEMM (solid lines:  $C = 0.25$ ; dashed lines:  $C = 0.36$ ; and dotted lines:  $C = 0.44$ ). The experimental data for Alq<sub>3</sub> is presented as red crosses [48] and red squares [46–50], while for  $\alpha$ -NPD it is shown as blue spheres [46,47] and triangles [51]. For  $\alpha$ -NPD, mobilities from fit-based GDM (green, dashed-dot-dot line) and correlated disorder model (CDM) (green, dashed-dashed-dot line) models [52] are additionally displayed.

in Alq<sub>3</sub> and  $\alpha$ -NPD as calculated with GEMM for  $C = 0.25, 0.36$ , and  $0.44$  (as in Fig. 2) as well as experimental values [46,48,51] and a fit based on analytical theories of van Mensfoort *et al.* [52]

The temperature dependence found in the GEMM with the effective-medium coefficient  $C = 0.25$  again agrees best with the experimental data for both Alq<sub>3</sub> and  $\alpha$ -NPD, both in terms of the absolute values and in the slope [the latter defined as  $m = \frac{\Delta \log_{10}(\mu_0)}{\Delta (1000/T)^2}$ , see Table I].

## IV. DISCUSSION

For the two model systems we are thus left with the puzzling observation that the experimental absolute values of the zero-field mobility and its temperature dependence are in better agreement with the original GEMM than with its modifications in the strong disorder limit where one would clearly expect the latter to be relevant.

As these observations result from the use of *ab initio* data for  $\sigma$ ,  $J$ , and  $\lambda$  with Marcus rates, it is instructive to turn the question around and to alternatively assume percolation transport and fit the microscopic parameters as is customary [52]. For example, in Ref. [48] the experimental

TABLE I. The slope  $m$  defined in the text calculated by the analytic expression Eq. (12) for three different  $C$  factors, listed in the first column, along with the experimental slopes.  $C = 0.25$  gives the best agreement with the experiment for both  $\alpha$ -NPD and Alq<sub>3</sub>.

	$m$ ( $\alpha$ -NPD)	$m$ (Alq <sub>3</sub> )
$C = 0.25$	−0.25	−0.77
$C = 0.36$	−0.36	−1.09
$C = 0.44$	−0.45	−1.35
Expt.	−0.14 to −0.18	−0.49

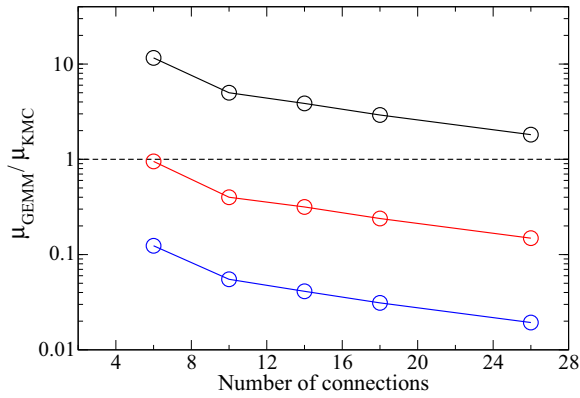


FIG. 4. (Color online) Ratio of zero-field mobilities obtained from GEMM and KMC for an SC lattice with disorder strength of  $\beta\sigma = 5$  (typical material with such disorder:  $\alpha$ -NPD) as function of the number of links (for each hopping site) for three values of  $C$  [see Eq. (12): 0.25 (black), 0.36 (red), and 0.44 (blue)]. As indicated by the dashed line, with an increased number of links the GEMM increasingly agrees with the KMC results. The opposite trend is observed for  $C = 0.36$  and 0.44 where the discrepancy increases.

temperature dependence of the zero-field mobility of  $\text{Alq}_3$  was well fitted by Eq. (2). However, the extracted value for the energy disorder  $\sigma_{\text{exp}} = 0.138$  eV was significantly smaller than what results from recent first-principles calculations of hole transport in  $\text{Alq}_3$  [14,16,20], which all yield values of  $\sigma \approx 0.2$  eV for uncorrelated energy disorder (in good agreement with photoluminescence measurements of  $\text{Alq}_3$  [53]). As the temperature dependence in all models is dominated by the exponential term in the mobility equation we thus find that the values of  $\sigma$  obtained by *ab initio* calculations seem to be at odds with exponents derived for lattice models with uncorrelated disorder.

How can this apparent discrepancy be dissolved? Bässler's exponent ( $C = 0.44$ ) is relevant for strong disorder or near the percolation limit [11], whereas the fitted exponent ( $C \sim 0.36$ ) is valid for medium disorder strengths as shown in prior works [41]. However, the agreement between the model using effective-medium exponents ( $C = 0.25$ ) and the experimental data is striking.

Closer inspection reveals one additional difference in the functional dependence of the GEMM and KMC models on the system parameters: In the GEMM, the dependence on the connectivity of the system, i.e., on the number of neighbors that can be reached from any given site ( $M$ ), is linear, whereas in percolative models there is a much stronger dependence. In the following we will, therefore, investigate a possibility to reconcile the apparently conflicting observations from microscopic analysis and fitted transport models.

By construction, the GEMM will deviate from the correct percolation limit as a function of  $\sigma$  (see Fig. 1), but the disorder threshold where this deviation becomes significant (say by one order of magnitude) depends strongly on the connectivity of the lattice as observed previously by Bässler [11]. In Fig. 4 we present KMC data for an SC lattice in which the connectivity of the lattice to next-nearest and next-next-nearest neighbors is progressively increased (for details, see Appendix D). As a result the crossover regime where the effective-medium theory

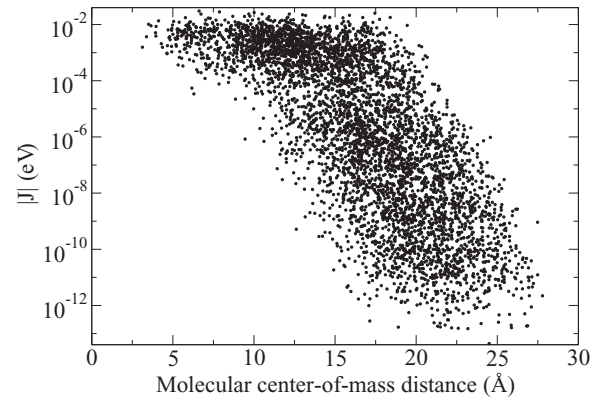


FIG. 5. Scatter plot of the logarithm of the absolute values of the transfer integrals as a function of intermolecular distance for  $\alpha$ -NPD. Although the linear behavior (exponential decay) is clearly observable, the spread indicates that an efficient connectivity exists until up to 20-Å (center-of-mass) distance between  $\alpha$ -NPD molecules.

strongly deviates from the percolation theory occurs at larger values of the disorder parameter. This is physically intuitive because increasing the number of connections in the lattice will dramatically affect the percolation threshold, which near to the percolation limit is dominated by the weakest bond in the system. If we consider an SC lattice with some particular percolation path, adding bonds in competition with the weakest nearest-neighbor bond will dramatically increase the mobility, whereas only a linear change is expected in the prefactor in Eq. (12) of the GEMM.

As Fig. 4 shows, the effective-medium model becomes relevant even for relatively large disorder  $\beta\sigma = 5$  as the connectivity of the model increases. In order to verify this for realistic bulk systems we have computed the distribution of hopping matrix elements for an  $\alpha$ -NPD morphology that was generated using molecular dynamics (see Appendix C) and subsequently analyzed with the quantum patch method [27] (Fig. 5). Although we find an exponential decay of the average hopping matrix element as a function of distance (representing an exponential decay of the mobility with decreasing hopping-site concentration), there is a significant spread of hopping matrix elements around the mean. In particular, large hopping matrix elements are found even at considerable distances among  $\alpha$ -NPD molecules (20-Å center-of-mass distance). This means that the number of connections, which dramatically affects mobility, has to be explicitly determined by microscopic calculations. Mapping such a realistic morphology on a lattice model might thus generate couplings that exceed the nearest-neighbor distance by far.

Ultimately, only KMC calculations on realistic morphologies will answer the question whether the effective increase in the connectivity will reconcile percolation theory with disorder parameters computed from *ab initio* methods. These calculations are nontrivial because it is presently not possible to generate realistic morphologies of sufficient size [24] to be directly used in KMC calculations. Recent work suggests [17,54] that there may exist effective mapping techniques that extrapolate parameters from small samples to sufficient

system size, but their viability for realistic systems has yet to be demonstrated.

We note that the decay of the zero-field hole mobility at lower temperatures is overestimated in the GEMM approach compared to the experimental values. Alq<sub>3</sub> has a significant molecular dipole moment ( $\sim 5$  D) so that it seems overly simplistic to neglect the energy correlations. In accordance with Ref. [52] where the CDM-based zero-field mobilities show a lower temperature slope than the uncorrelated GDM, we suspect this to be the prime reason for the rather steep GEMM slopes in Fig. 3. Inclusion of energy correlations as in Ref. [52] is the next natural step in the refinement of the method and as such will be addressed in the near future.

We further note that the presented analytic model is reminiscent of the mean-medium approximation (MMA) developed by Shaked *et al.* [55], Roichman *et al.* [56], Roichman [57], and Tessler *et al.* [58] as a practical method to model semiconductor devices. The MMA was applied to calculate the charge-carrier mobilities in organic semiconductors having Gaussian DOS. Its main approximation is the assumption that the whole spectrum of energies, distributed with the DOS probability function, is accessible from each site. This transforms the master-equation-on-lattice problem into a continuum-mean-medium problem. One of the drawbacks of this continual mapping is the loss of the exponential dependence of the mobility on the hopping site concentration and temperature, which is avoided in the present model. These dependencies are fully preserved in the GEMM as readily displayed in Fig. 5, i.e., the dependence of  $J$  on intermolecular distance corresponds to the mobility dependence on the hopping-site concentration. Likewise, as shown in Fig. 3, the temperature dependence of the GEMM mobility Eq. (12) for  $\alpha$ -NPD is somewhere between the GDM and the CDM [52]. The assumption of the MMA, that the charge-carrier distribution in the steady state can be described by the equilibrium Fermi-Dirac distribution function, is similar to our use of the equilibrium charge distribution at  $t = 0$  in the derivation in Sec. II B. The MMA can obviously provide only the upper limit of the possible current for a given DOS (as each site contains all possible energies, the fastest transfer process determines the current), in analogy to what applies for the GEMM. In the limit of low carrier concentration, both approaches result in the exponent  $C = 0.25$  for a Gaussian DOS [12,59]. At this point, however, the similarity between the methods ceases to hold as the GEMM allows one to account for possible correlations between site energies and transfer integrals, which seems not to be possible in the MMA.

Finally, in contrast to Refs. [43–45], we use here model parameters obtained by *ab initio* methods, including explicit small-molecule morphology simulations. Use of these parameters allows us to separate the dependence of the mobility in terms of the prefactor of  $\sigma$  in the exponent from the other input data. For example, if we consider the results presented in Fig. 7 in Ref. [45], we find  $C = 0.41$  for  $4\sigma/\lambda = 3.3$  (the value which corresponds to  $\alpha$ -NPD), whereas we have shown in this paper that  $C = 0.25$  best reproduces the experimental values across the complete temperature range. This suggests that a third dimension to the parametric space of  $C$  vs  $\sigma/E_a$ , e.g., the effective connectivity of the hopping sites, might be necessary to accurately capture involved physics. We note that

$C = 0.25$  is a solid limit of the GEMM in full agreement with the KMC results from Ref. [45], demonstrating the validity of the GEMM in the small disorder limit.

To summarize, we have developed a GEMM that provides an analytic approach to compute the zero-field mobility in disordered organic semiconductors based on *ab initio* data from microscopic theory. By fitting to lattice KMC data we have extended this model to the percolation limit but found for two realistic systems that the experimental data are better described by the original effective-medium exponent than by its percolationlike modifications. As a possible explanation for this apparent discrepancy we suggest that the connectivity of a realistic morphology when mapped onto a lattice model may be larger than what is assumed in systems used to parametrize percolation theory. Finally, we believe that much insight can be gained from the availability of analytic models, which yield a functional dependence of the mobility on the system parameters without necessarily requiring excessive computational resources.

## ACKNOWLEDGMENT

The authors acknowledge financial support from the EU FP7 Project MMM@HPC (No.261549) and the joint STN-DFG Project MODEOLED.

## APPENDIX A: DERIVATION OF EQ. (6) FROM EQ. (5)

In the zero-field limit the following expression for the mobility tensor  $\mu^{\alpha\gamma}$ ,  $v^\alpha = \mu^{\alpha\gamma} F_\gamma$ , can be derived from Eq. (5):

$$\mu^{\alpha\gamma} = \frac{1}{2N_c} \sum_{ij} \Gamma_{ij}^{(0)} \left( \frac{1}{\omega_{ji}^{(0)}} \frac{\partial \omega_{ji}}{\partial F_\gamma} - \frac{1}{\omega_{ij}^{(0)}} \frac{\partial \omega_{ij}}{\partial F_\gamma} \right) r_{ij}^\alpha. \quad (\text{A1})$$

One can proceed further with an analytical derivation, if a general representation for the transition rates  $\omega_{ij} = A_{ij} \varphi(\epsilon_{ij}^-)$  is assumed, with  $\epsilon_{ij}^+ = (\epsilon_i + \epsilon_j)/2$ ,  $\epsilon_{ij}^- = (\epsilon_i - \epsilon_j)/2$  being the mean energy and the energy difference of the neighboring sites, respectively. The coefficients  $A_{ij}$  are constants. The function  $\varphi(\epsilon_{ij}^-)$  depends on the external field only through the change in the energy difference  $\epsilon_{ij}^- \rightarrow \epsilon_{ij}^- + \delta_F \epsilon_{ij}^-$  induced by the field. Then  $\frac{\partial \omega_{ij}}{\partial F_\gamma} = \frac{\partial \omega_{ij}^{(0)}}{\partial \epsilon_{ij}^-} \frac{\partial \delta_F \epsilon_{ij}^-}{\partial F_\gamma}$ , and by once more using the detailed balance condition one gets

$$\mu^{\alpha\gamma} = \frac{1}{2N_c} \sum_{ij} \Gamma_{ij}^{(0)} \left( -2\beta \frac{\partial \delta_F \epsilon_{ij}^-}{\partial F_\gamma} \right) r_{ij}^\alpha. \quad (\text{A2})$$

By neglecting fluctuations in the induced local electric field,  $\delta_F \epsilon_i = -q(\vec{F}\vec{r}) - (\vec{F}\vec{d}_i)$ , where  $\vec{d}_i$  is the dipole moment of the site  $i$ ,  $q = \pm e$  is the charge of the carrier, and one finally arrives at Eq. (6),

$$\mu^{\alpha\gamma} = \frac{q\beta}{2N_c} \sum_{ij} \Gamma_{ij}^{(0)} r_{ij}^\alpha (r_{ij}^\gamma + d_{ij}^\gamma/q) \quad (\text{A3})$$

To derive the final expression (12) for the mobility in the zero-field and low-concentration limit from Eq. (11), the following averages for the Gaussian density of states have been

used (assuming no correlations in the site energies);

$$\langle e^{-\beta\epsilon} \rangle = \frac{1}{\sqrt{2\pi\sigma}} \int \exp\left[-\frac{\epsilon^2}{2\sigma^2} - \beta\epsilon\right] d\epsilon = e^{(\beta\sigma)^2/2},$$

$$\langle e^{-\beta\epsilon^+} \rangle = e^{(\beta\sigma)^2/4} \quad \text{and} \quad \langle e^{-\beta(\epsilon^-/\lambda)} \rangle = \left(1 + \frac{\beta\sigma^2}{\lambda}\right)^{-1/2}. \quad (\text{A4})$$

## APPENDIX B: DERIVATION OF ACCELERATION OF CHARGE CARRIERS AT $t = 0$

Here we are going to calculate the acceleration of charge carriers at  $t = 0$ . A formal solution of the linearized ME  $\frac{d\vec{p}}{dt} = \hat{\Omega}\vec{p}$  can be written as

$$\vec{p}(t) = \vec{p}_\infty + \exp(\hat{\Omega}t)(\vec{p}_0 - \vec{p}_\infty) = \vec{p}_\infty + \exp(\hat{\Omega}t)\vec{p}_0, \quad (\text{B1})$$

where  $\hat{\Omega}_{ij} = \omega_{ji} - \delta_{ij} \sum_{j' \neq i} \omega_{ij'}$  is the matrix of transition rates,  $\vec{p}(t)$  is a vector of the occupation probabilities,  $\vec{p}(t = 0) = \vec{p}_0$ , and  $\vec{p}(t = \infty) = \vec{p}_\infty$ . By  $t = \infty$  the system has relaxed to a new thermal equilibrium state, therefore  $\hat{\Omega}\vec{p}_\infty = 0$ .

Directly from Eq. (B1) follow general expressions for the mean charge velocity  $\vec{v}(t) = \vec{R}^T \exp(\hat{\Omega}t)\hat{\Omega}\vec{p}_0$  and the mean acceleration  $\vec{a}(t) = \vec{R}^T \exp(\hat{\Omega}t)\hat{\Omega}^2\vec{p}_0$  as functions of time with  $\vec{R}^T = (\vec{r}_1, \dots, \vec{r}_N)$  being the vector of site coordinates.

At  $t = 0$  and for weak fields the projection of the acceleration onto the field direction becomes

$$\vec{F}\vec{a}(0) = -2q\beta \sum_i \left[ \sum_j (\vec{F}\vec{r}_{ij}) \bar{\omega}_{ij} e^{-\beta(\epsilon_j - \mu)/2} \right]^2, \quad (\text{B2})$$

where  $\bar{\omega}_{ij}$  is the symmetric part of the hopping rate:  $\bar{\omega}_{ij} = \omega_{ij} e^{-\beta\epsilon_{ij}^{(-)}}$ . This clearly shows that the charge is being decelerated at  $t = 0$ , unless the sum in brackets vanishes for all sites (that is the case, e.g., for a regular cubic lattice of sites with no energetic disorder).

## APPENDIX C: CALCULATION OF MICROSCOPIC PARAMETERS

A morphology of 300  $\alpha$ -NPD molecules was generated with the molecular dynamics package GROMACS [60]. After equilibration at 850 K for 1 ns, the system was cooled down to 300 K with a cooling rate of 200 K/ns and finally equilibrated for 1 ns at a constant pressure of 1 bar. The general amber force field [61] with Austin Model 1-bond-charge-correction partial charges [62,63] was used for the calculations. The molecule topologies and parameters are generated with the ACPYPE tool [64]. To converge electrostatics

in the subsequent quantum mechanical calculations the cell was further periodically extended to 8100 molecules. The inner part of the morphology, which was used to extract microscopic parameters (100 molecules), was postrelaxed using the density functional theory package TURBOMOLE with the Becke three-parameter Lee-Yang-Parr hybrid functional and def2-SV(P) basis functions. The molecules were thereby relaxed individually in their immediate and fixed environment.

For Alq<sub>3</sub>, a morphology generated with the VOTCA [16,65] package was used. It contains 512 molecules and was periodically extended to 13 824 molecules in order to reach convergence for long-range electrostatic interaction. Energy disorder and transfer integrals were obtained utilizing the quantum patch method [27], which equilibrates the charge densities of the molecules in the morphology. The reorganization energy was calculated based on the four-point procedure of Nelson and co-workers [66,67], which limits the  $\lambda$  calculation to the inner part only. The impact of environment is modeled through limiting relaxations of dihedral angles. Namely, for many of the molecules the dihedral angles are changing quite dramatically upon charging and relaxation in vacuum. Such a severe change in dihedral angle will hardly be possible in any realistic morphology [68]. As such, we have restricted our calculations to the ‘‘frozen dihedral approximation’’ where we relax all the other degrees of freedom upon charging except the aforementioned dihedrals, which are kept fixed.

## APPENDIX D: LATTICE CONNECTIVITY IN CUBIC LATTICES

To simulate charge transport in lattice topologies with varying connectivity  $M$ , we partition the system in the nearest-neighbor (further abbreviated as n-n), the second n-n, and the third n-n shells. For the first n-n (6 sites) shell a connectivity of 6 is given by the six equal transfer integrals  $J_{if}^{1n} = e^{-\alpha R_{if}}$ , whereas, at the same time, in the second n-n shell (sites 7 to 18) and the third n-n shell (sites 19 to 26) the transfer integrals are set to  $J_{if}^{2n} = J_{if}^{3n} = 0$ . To gradually increase the connectivity from the first n-n shell to the second ( $M = 6$  to  $6 < M \leq 18$ ) without introducing off-diagonal disorder in the SC topology, we increase the transfer integrals in the second n-n shell according to  $J_{if}^{2n} = J_{if}^{1n} (M - 6)/12$ , keeping  $J_{if}^{3n} = 0$  in the third. This effectively corresponds to  $M$  connections/hopping channels with a transfer integral of  $J_{if}^{1n}$ . The former equivalence is valid if the external electric field in the KMC simulations is applied along the  $z$  axis of the SC lattice such that the potential drop due to the field as well as the hopping distance in the field direction is identical for all 26 sites. Similarly, when further extending the connectivity to the third n-n shell ( $18 < M \leq 26$ ) we additionally set all  $J_{if}^{3n}$  to  $J_{if}^{3n} = J_{if}^{1n} (M - 18)/8$ .

- [1] L. S. Hung and C. H. Chen, *Mater. Sci. Eng., R* **39**, 143 (2002).  
 [2] B. Kippelen and J.-L. Bredas, *Energy Environ. Sci.* **2**, 251 (2009).  
 [3] A. W. Hains, Z. Liang, M. A. Woodhouse, and B. A. Gregg, *Chem. Rev.* **110**, 6689 (2010).

- [4] C. D. Dimitrakopoulos and P. R. L. Malenfant, *Adv. Mater.* **14**, 99 (2002).  
 [5] B. Baumeier, F. May, C. Lennartz, and D. Andrienko, *J. Mater. Chem.* **22**, 10971 (2012).  
 [6] M. Mesta *et al.*, *Nat. Mater.* **12**, 652 (2013).  
 [7] N. Karl, *Mol. Cryst. Liq. Cryst.* **171**, 31 (1989).

- [8] S. M. Sze and K. K. Ng, *Physics of Semiconductor Devices*, 3rd ed. (Wiley, New York, 2006).
- [9] Y. Shirota, *J. Mater. Chem.* **15**, 75 (2005).
- [10] Y. Shirota and H. Kageyama, *Chem. Rev.* **107**, 953 (2007).
- [11] H. Bässler, *Phys. Status Solidi B* **175**, 15 (1993).
- [12] W. F. Pasveer, J. Cottaar, C. Tanase, R. Coehoorn, P. A. Bobbert, P. W. M. Blom, D. M. de Leeuw, and M. A. J. Michels, *Phys. Rev. Lett.* **94**, 206601 (2005).
- [13] V. Coropceanu, J. Cornil, D. A. da Silva Filho, Y. Olivier, R. Silbey, and J.-L. Brédas, *Chem. Rev.* **107**, 926 (2007).
- [14] J. Kwiatkowski, J. Nelson, H. Li, J. Bredas, W. Wenzel, and C. Lennartz, *Phys. Chem. Chem. Phys.* **10**, 1852 (2008).
- [15] A. Lukyanov, C. Lennartz, and D. Andrienko, *Phys. Status Solidi A* **206**, 2737 (2009).
- [16] V. Rühle, A. Lukyanov, F. May, M. Schrader, T. Vehoff, J. Kirkpatrick, B. Baumeier, and D. Andrienko, *J. Chem. Theory Comput.* **7**, 3335 (2011).
- [17] B. Baumeier, O. Stenzel, C. Poelking, D. Andrienko, and V. Schmidt, *Phys. Rev. B* **86**, 184202 (2012).
- [18] Y. Nagata and C. Lennartz, *J. Chem. Phys.* **129**, 034709 (2008).
- [19] A. Lukyanov and D. Andrienko, *Phys. Rev. B* **82**, 193202 (2010).
- [20] A. Fuchs, T. Steinbrecher, M. S. Mommer, Y. Nagata, M. Elstner, and C. Lennartz, *Phys. Chem. Chem. Phys.* **14**, 4259 (2012).
- [21] V. Ambegaokar, B. I. Halperin, and J. S. Langer, *Phys. Rev. B* **4**, 2612 (1971).
- [22] S. Kirkpatrick, *Rev. Mod. Phys.* **45**, 574 (1973).
- [23] M. C. J. M. Vissenberg and M. Matters, *Phys. Rev. B* **57**, 12964 (1998).
- [24] J. Cottaar, L. J. A. Koster, R. Coehoorn, and P. A. Bobbert, *Phys. Rev. Lett.* **107**, 136601 (2011).
- [25] J. J. M. van der Holst, F. W. A. van Oost, R. Coehoorn, and P. A. Bobbert, *Phys. Rev. B* **83**, 085206 (2011).
- [26] J. Cottaar, Ph.D. thesis, Eindhoven University of Technology, 2012.
- [27] P. Friederich, F. Symalla, V. Meded, T. Neumann, and W. Wenzel, *J. Chem. Theory Comput.* **10**, 3720 (2014).
- [28] A. Miller and E. Abrahams, *Phys. Rev.* **120**, 745 (1960).
- [29] F. May, B. Baumeier, C. Lennartz, and D. Andrienko, *Phys. Rev. Lett.* **109**, 136401 (2012).
- [30] S. D. Baranovskii, H. Cordes, F. Hensel, and G. Leising, *Phys. Rev. B* **62**, 7934 (2000).
- [31] V. I. Arkhipov, E. V. Emelianova, and G. J. Adriaenssens, *Phys. Rev. B* **64**, 125125 (2001).
- [32] L. Li, G. Meller, and H. Kosina, *J. Appl. Phys.* **106**, 013714 (2009).
- [33] V. Stehr, J. Pfister, R. F. Fink, B. Engels, and C. Deibel, *Phys. Rev. B* **83**, 155208 (2011).
- [34] T. Kasuya, *J. Phys. Soc. Jpn.* **13**, 1096 (1958).
- [35] S. Marianer and B. I. Shklovskii, *Phys. Rev. B* **46**, 13100 (1992).
- [36] V. Capek, *Phys. Rev. B* **36**, 7442 (1987).
- [37] W.-Q. Deng and W. A. Goddard, *J. Phys. Chem. B* **108**, 8614 (2004).
- [38] C. Lee, R. Waterland, and K. Sohlberg, *J. Chem. Theory Comput.* **7**, 2556 (2011).
- [39] R. A. Marcus, *Rev. Mod. Phys.* **65**, 599 (1993).
- [40] X. Feng, V. Marcon, W. Pisula, M. R. Hansen, J. Kirkpatrick, F. Grozema, D. Andrienko, K. Kremer, and K. Mullen, *Nat. Mater.* **8**, 421 (2009).
- [41] J. Cottaar, R. Coehoorn, and P. A. Bobbert, *Phys. Rev. B* **85**, 245205 (2012).
- [42] B. Movaghar and W. Schirmacher, *J. Phys. C: Solid State Phys.* **14**, 859 (1981).
- [43] P. Parris, V. M. Kenkre, and D. H. Dunlap, *Phys. Rev. Lett.* **87**, 126601 (2001).
- [44] I. I. Fishchuk, A. Kadashchuk, H. Bässler, and S. Nešpurek, *Phys. Rev. B* **67**, 224303 (2003).
- [45] I. I. Fishchuk, A. Kadashchuk, S. T. Hoffmann, S. Athanasopoulos, J. Genoe, H. Bässler, and A. Köhler, *Phys. Rev. B* **88**, 125202 (2013).
- [46] S. Naka, H. Okada, H. Onnagawa, Y. Yamaguchi, and T. Tsutsui, *Synth. Met.* **111-112**, 331 (2000).
- [47] S. C. Tse, K. C. Kwok, and S. K. So, *Appl. Phys. Lett.* **89**, 262102 (2006).
- [48] H. H. Fong and S. K. So, *J. Appl. Phys.* **100**, 094502 (2006).
- [49] R. G. Kepler, P. M. Beeson, S. J. Jacobs, R. A. Anderson, M. B. Sinclair, V. S. Valencia, and P. A. Cahill, *Appl. Phys. Lett.* **66**, 3618 (1995).
- [50] J. Kalinowski, N. Camaioni, P. Di Marco, V. Fattori, and A. Martelli, *Appl. Phys. Lett.* **72**, 513 (1998).
- [51] C. H. Cheung, K. K. Tsung, K. C. Kwok, and S. K. So, *Appl. Phys. Lett.* **93**, 083307 (2008).
- [52] S. L. M. van Mensfoort, V. Shabro, R. J. de Vries, R. A. J. Janssen, and R. Coehoorn, *J. Appl. Phys.* **107**, 113710 (2010).
- [53] E. W. Forsythe, D. C. Morton, and D. Chiu, *SID Int. Symp. Dig. Tech. Pap.* **33**, 1266 (2002).
- [54] P. Kordt, O. Stenzel, B. Baumeier, V. Schmidt, and D. Andrienko, *J. Chem. Theory Comput.* **10**, 2508 (2014).
- [55] S. Shaked, S. Tal, Y. Roichman, A. Razin, S. Xiao, Y. Eichen, and N. Tessler, *Adv. Mater. (Weinheim, Ger.)* **15**, 913 (2003).
- [56] Y. Roichman, Y. Preezant, and N. Tessler, *Phys. Status Solidi A* **201**, 1246 (2004).
- [57] Y. Roichman, Ph.D. thesis, Technion-Israel Institute of Technology, Faculty of Electrical Engineering, 2004.
- [58] N. Tessler, Y. Preezant, N. Rappaport, and Y. Roichman, *Adv. Mater. (Weinheim, Ger.)* **21**, 2741 (2009).
- [59] R. Coehoorn, W. F. Pasveer, P. A. Bobbert, and M. A. J. Michels, *Phys. Rev. B* **72**, 155206 (2005).
- [60] S. Pronk *et al.*, *Bioinformatics* **29**, 845 (2013).
- [61] J. Wang, R. M. Wolf, J. W. Caldwell, P. A. Kollman, and D. A. Case, *J. Comput. Chem.* **25**, 1157 (2004).
- [62] A. Jakalian, B. L. Bush, D. B. Jack, and C. I. Bayly, *J. Comput. Chem.* **21**, 132 (2000).
- [63] A. Jakalian, D. B. Jack, and C. I. Bayly, *J. Comput. Chem.* **23**, 1623 (2002).
- [64] A. W. S. da Silva and W. F. Vranken, *BMC Res. Notes* **5**, 367 (2012).
- [65] V. Rühle, C. Junghans, A. Lukyanov, K. Kremer, and D. Andrienko, *J. Chem. Theory Comput.* **5**, 3211 (2009).
- [66] S. F. Nelsen, S. C. Blackstock, and Y. Kim, *J. Am. Chem. Soc.* **109**, 677 (1987).
- [67] S. F. Nelsen, M. N. Weaver, Y. Luo, J. R. Pladziewicz, L. K. Ausman, T. L. Jentzsch, and J. J. O'Konek, *J. Phys. Chem. A* **110**, 11665 (2006).
- [68] H. Li, L. Duan, D. Zhang, and Y. Qiu, *J. Phys. Chem. C* **118**, 14848 (2014).